Energy & Environmental Science

Probing Microstructure and Electrolyte Concentration Dependent Cell Chemistry via Operando Small Angle Neutron Scattering

Journal:	*Energy & Environmental Science*
Manuscript ID	EE-ART-09-2018-002703.R3
Article Type:	Paper
Date Submitted by the Author:	24-Jan-2019
Complete List of Authors:	Jafta, Charl; Oak Ridge National Laboratory, Chemical Science Division Sun, Xiao-Guang; Oak Ridge National Laboratory, Chemical Science Division Veith, Gabriel; Oak Ridge National Laboratory, Materials Science and Technology Division Jensen, Grethe; University of Delaware, Chemical Engineering; Mahurin, Shannon; Oak Ridge National Lab, Paranthaman, Mariappan; Oak Ridge National Laboratory, Chemical Sciences Division Dai, Sheng; Oak Ridge National Laboratory, Bridges, C. A.; ORNL, Chemical Sciences Division

Probing Microstructure and Electrolyte Concentration Dependent Cell Chemistry via Operando Small Angle Neutron Scattering

Charl J. Jafta[*a], Xiao-Guang Sun[a], Gabriel M. Veith[b], Grethe V. Jensen[c], Shannon M. Mahurin[a], Mariappan P. Paranthaman[a], Sheng Dai[a] and Craig A. Bridges[*a]

[a]Chemical Sciences Division and [b]Materials Science and Technology Division, Oak Ridge National Laboratory, Oak Ridge, Tennessee 37831, United Sates
[c]Center for Neutron Research, National Institute of Standards and Technology, Gaithersburg, Maryland 20899, United States

The key to understanding the cycling mechanism of lithium-ion battery electrodes is to develop methods to monitor the dynamic cell chemistry, but the complexity of the problem has continued to pose an obstacle. Here we describe the use of *operando* small-angle neutron scattering (SANS) to show directly how the use of concentrated LiTFSI electrolyte in Li/ordered mesoporous carbon (OMC) half-cells influences the mechanism of solid electrolyte interphase (SEI) formation, lithium intercalation, and carbon framework expansion. We find that a complex interplay between the viscosity, lithium solvation shell and electrode microstructure in the concentrated 4M electrolyte changes the dynamics of SEI formation and pore filling at a given applied potential. Both the filling of micropores and co-intercalation are found to drive the expansion of the carbon framework. Lithium-rich reduction products form at much higher potentials in the micropores of the 4M electrolyte system, while on mesopore surfaces the lithium-rich salts form quickly before giving way to carbonaceous products. This study reveals *operando* SANS as a unique method for providing microstructure dependent information on the dynamics of electrochemical processes.

Introduction

With the ever-increasing world population and the use of smart technologies for everyday purposes becoming a norm, there is an increased demand for longer lasting, faster charging and safer batteries. With this in mind, research related to the development of new types of carbon electrodes[1-3] and electrolytes[4] remains a key area of focus for battery researchers. The central role of the electrolyte in performance and safety [5, 6] has led to the development of ionic liquid, organosilicon, fluoroether, and solid state alternatives, all with tradeoffs on viscosity, electrochemical stability and conductivity. The choice of salt for the electrolyte is similarly important, and the standard $LiPF_6$ salt is a compromise amongst other commercially available Li salts each with too many potential disadvantages, such as toxicity, an unstable or uneven passivation layer, high corrosion of the current collector, or poor conductivity [7]. Replacing $LiPF_6$ with $LiN(SO_2CF_3)_2$ (LiTFSI) can improve thermal and chemical stability of the electrolyte [8, 9], but can result in Al corrosion at high voltages [10, 11]. However, Matsumoto et al. successfully suppressed Al corrosion using high LiTFSI concentration in the electrolyte[12]. Increasing the solution concentration may enable new cell chemistry for carbonate electrolytes, as well as the development of beyond lithium ion battery chemistries[13, 14]. Reversible Li^+ intercalation has been shown for concentrated propylene carbonate(PC)-based electrolytes in graphite based half-cells without exfoliation [15-17], and higher concentration electrolytes could suppress lithium dendrite formation and potentially enable Li metal as an anode material [18, 19]. Despite these promising results, it remains challenging to understand the mechanism by which these new chemistries achieve higher performance. As compared to a typical dilute (ca. < 3 M [mol/L]) electrolyte system in which the salt (i.e. LiTFSI) cations (Li^+) are coordinated with 3 to 4 solvent molecules (i.e. $Li^+(PC)_4$) [20], a 4 M LiTFSI/PC electrolyte solution has a PC:Li ratio of 0.4:1 that results in ion association to form Li^+(PC)-

TFSI aggregates. The increased ion association results in formation of contact ion pairs (CIPs) and aggregates (AGGs) [6, 21-23]. Reports suggest that the $TFSI^-$ anions in the CIPs and AGGs are sacrificially reduced to form a stable passivating layer that is rich in LiF [17, 24-28]. It is reported that the LiF based solid electrolyte interphase (SEI) is superior in adhesion to the electrode surface, and thinner and denser with superior mechanical properties [29, 30]. Given the importance of the inorganic salt layer, a key question is therefore to understand how this change in the cation (Li^+) coordination with concentration of LiTFSI, along with the increase in electrolyte viscosity, influences the formation of inorganic salt products (i.e., LiF, LiOH) versus carbonaceous products [9, 31] in the SEI during the critical initial discharge cycle.

In this work, we compare the evolution in surface chemistry and electrode microstructure for dilute and concentrated LiTFSI/PC electrolytes on mesoporous hard carbon, using an *operando* small-angle neutron scattering (SANS) cell design (**Fig. 1a**) that provides an exceptional level of mechanistic information during the initial discharge. *Operando* methods have been used to study the lithiation mechanism for dilute solution in graphite [32-35], and hard carbon (HC) [36-38], as well as small-angle X-ray Scattering (SAXS) and *ex situ* SANS [37, 39]. From this, several concepts on the cycling mechanism have been proposed. In particular for HC, it has been suggested that Li will form metal clusters in nanovoids formed by the random stacking of graphitic domains [40]. The lithiation mechanism was proposed to have lithium insertion into graphitic layers at higher voltage, followed by insertion into nanovoids (micropores) at lower voltage, but there is limited data on how the cell chemistry may change with voltage. There has remained uncertainty as to whether co-intercalation of PC molecules occurs in concentrated electrolytes; one *operando* AFM study [15] with concentrated LiTFSI/PC found no evidence of co-intercalation of PC molecules, while another suggested co-intercalation occurs[41]. In terms of the surface chemistry, X-ray photoelectron spectroscopy (XPS) has been used [17, 26, 30] to characterize graphite electrodes *ex situ* after immersion into the concentrated electrolytes (before) and after a discharge-charge cycle (after) by XPS, and *operando* AFM was employed in order to study SEI film evolution [15, 23, 41]. Thus, these studies have provided a basis for understanding the lithiation mechanism and the structure of carbon but are missing key details of how the SEI composition evolves during the discharge as a function of concentration. It has been shown that *operando* SANS is a powerful technique to study the evolution of the SEI during the first lithiation process as well as the accompanied framework expansion dynamics of hard carbon (HC) [42, 43]. We show here that *operando* SANS, in combination with *ex-situ* XPS data collected at selected potentials, provides unprecedented detail on the concentration dependent filling of mesopores and micropores with Li-rich and carbonaceous products, co-intercalation of solvated Li^+, and corresponding electrode microstructure expansion during the initial discharge process. This highlights the critical importance of considering the relationship between microstructure, viscosity and concentration on cell chemistry when developing new electrolytes.

Experimental

Materials. The Ordered mesoporous carbon (OMC) powder was synthesized using a hard-templated method, as previously reported, and used as the active material in the electrode [44, 45]. The ordered and porous structure of the OMC was determined from TEM images and N_2 sorption isotherms obtained from a microscope and a Micrometrics Tristar 3000 nitrogen sorption analyzer, respectively.

Electrochemical Measurements. The OMC electrodes were obtained by mixing OMC (80 wt.%), carbon black (5 wt.%) and PVdF (15 wt.%) in N-methyl-2-pyrrolidon (NMP) into a well homogenized

slurry. The slurry was cast onto a Cu foil by doctor blade and left under a UV light to allow for solvent evaporation, after which the electrodes were placed in a vacuum oven overnight at 100 °C. The electrodes were pressed under a hydrolytic pressure of 3 ton for 1 min, cut into 1.3 cm^2 (Ø ≈ 1.3 cm) discs and transferred to an Ar filled glovebox. The active material loading of each electrode was approximately 2 mg/cm^2. Electrodes from the same batch were used for the SANS, XPS and EIS experiments. Two electrolytes of different concentrations were prepared in a glovebox by dissolving 1 M and 4 M LiTFSI in pure PC to obtain diluted and concentrated electrolytes, respectively. The 1 M and 4 M LiTFSI / PC electrolytes have viscosities of 6.25 cP and 167.3 cP, respectively, at 293 K. To put this in context, the viscosity of the common electrolyte 1M $LiPF_6$ / EC / EMC is ~2 cP, and the viscosity of pure PC is 2.5 cP (at RT), whereas the high concentration results in a much higher viscosity.

Electrode Characterization. For XPS measurements, two sets of coin cells (CR2032) were assembled with 1 M and 4 M electrolyte, respectively, and left for 24 h for electrolyte equilibration. Two of the cells, one from each concentration, 1M and 4M with open circuit voltages (OCV) at ~ 2.5 V and 2.9 V, respectively, were disassembled. The other cells were discharged, at a current density of 50 mA/g resulting in an absolute current of ~ 50 μA, to 1.1 V, 0.9 V, 0.3 V and 0.005 V and then disassembled, for each concentration. The cell disassembling was performed in an Ar filled glovebox. The OMC electrodes were washed with DMC, to remove excess salt and electrolyte, and directly transferred to a transfer vessel, which was used to transfer the samples to the ultra-high vacuum (UHV) chamber of the PHI 3056 XPS instrument. The spectra were obtained using an Al anode source operated at 15 kV for an applied power of 300 W. Survey scans were collected with a pass energy of 93.5 eV and the high-resolution spectra with a pass energy of 23.5 eV. Charge correction was done by shifting all the peaks relative to the C-C peak at a binding energy of 284.8 eV. All the XPS spectra were fitted using CasaXPS.

The *in-situ* Electrochemical Impedance Spectroscopy (EIS) was done using a Gamry Ref 3000 potentiostat capable of discharging and charging with intermittent potentiostatic EIS (pEIS, during potential hold). The pEIS was measured in the frequency range 1MHz to 100 mHz with an applied root mean square voltage amplitude of 10 mV. The pEIS experiment was designed to have similar parameters as the *operando* SANS experiment, with the electrodes having exactly the same active mass loading and cells discharged with a current of 50 μA. The pEIS was conducted at equi-coulombic steps of 120 mC, with each pEIS taking approximately 10 min to complete. The measured impedance spectra, as a function of the discharge at specific voltages as shown in **Fig. S7**, were fit with an electrochemical equivalent circuit (EEC) using the software ZFit.

***Operando* SANS data collection and evaluation.** The *operando* cell depicted in **Fig. 1a**, has an outer diameter of 28 mm, ideal for fitting in typical sample environments designed for SANS. The outer casing is TiZr windows which is alloyed in a ratio that will result in zero coherent scattering and also ensures a relatively high transmission (> 90%) of neutrons [46]. SANS measurements were carried out on the NGB 30m SANS instrument at the National Institute of Standards and Technology in Gaithersburg, MD [47]. SANS measurements were obtained as the cells were discharging / charging with a data accumulation time of 20 minutes. During the initial discharge absolute currents of 50 μA, 100 μA and 150 μA were used for the 1 M electrolyte system, whereas for the 4 M electrolyte system 50 μA and 100 μA were used. The subsequent cycles were charged / discharged at 150 μA and 100 μA for the 1 M and 4 M electrolyte systems, respectively. These currents were selected to optimize the information obtained from the neutron data collection, as detailed further in the supporting information and **Fig. S5**. The single scattering curves for the 1 M and 4 M cells at OCV, respectively,

are shown in **Fig. S2b** where the Bragg peaks indicate a well-ordered structure with a unit cell ($a_0 = 2d_{100}/\sqrt{3}$) of ~ 104 Å (~ 0.07 Å^{-1}), prior to cycling. The sample detector distance was 1 m with a collimation of 2 m and the wavelength used was $\lambda = 6$Å that yielded a total momentum transfer ($q = 4\pi \sin\theta/\lambda$) range of 0.03 Å$^{-1} \leq q \leq 0.5$ Å^{-1} where θ is the scattering angle.

Results and Discussion

Electrochemical performance in concentrated electrolyte system

The microstructure of these OMC carbons was selected to have a pore-pore spacing of ~10 nm, as shown by TEM in the inset of **Fig. S2**. The average pore size of ~4 nm was confirmed by BET analysis, with additional micropores below 2 nm indicated by the shape of the N_2 adsorption isotherm at low relative pressure. Furthermore, the adsorption data suggest a surface area of 702 m^2/g. The *ex situ* electrochemical data for the OMC carbons with 1 M and 4 M LiTFSI in PC display a large irreversible capacity in the first cycle, as expected for high surface area carbon in carbonate electrolytes (**Fig. S3**)[48]; the high surface area provides a sufficient signal for tracking the changes in surface chemistry using *operando* neutron scattering. The irreversible capacity at a rate of 50 mA/g rapidly fades in subsequent cycles to near 800 mAh/g and 400 mAh/g, for 1 M and 4 M cells, respectively (**Fig. S4a**). While the capacity of 4 M cell remains relatively constant over 100 cycles, the capacity of 1M gradually decreases. Similar relative capacities are seen at higher cycling rates for these concentrations (**Fig. S4b**). Whereas graphite electrodes with 1 M LiTFSI in PC show a voltage plateau near 0.8V consistent with exfoliation of graphene layers [15, 16], and graphite displays reversible cycling in high concentration electrolytes due to a passivation layer, the hard carbon cannot be exfoliated in the 1 M or 4 M electrolytes. This provides an opportunity to examine the chemistry of 1 M against 4 M electrolytes over the entire voltage range, using both *operando* and *ex situ* methods. The higher relative capacity for the 1 M cell over many cycles is consistent with a higher degree of intercalation for the 1M cell, as influenced by the diffusion limitations of the more viscous 4 M electrolyte, whereas the more stable cycling and higher efficiency of the 4 M cell reflects the more stable SEI formed by the concentrated electrolyte.

Voltage dependence of electrode chemistry in 1M and 4M electrolytes

To understand the observed performance differences as a function of electrolyte concentration, we probed the dynamic evolution of carbon microstructure and surface chemistry during cycling using *operando* measurements on the NGB 30m SANS beamline at NIST.

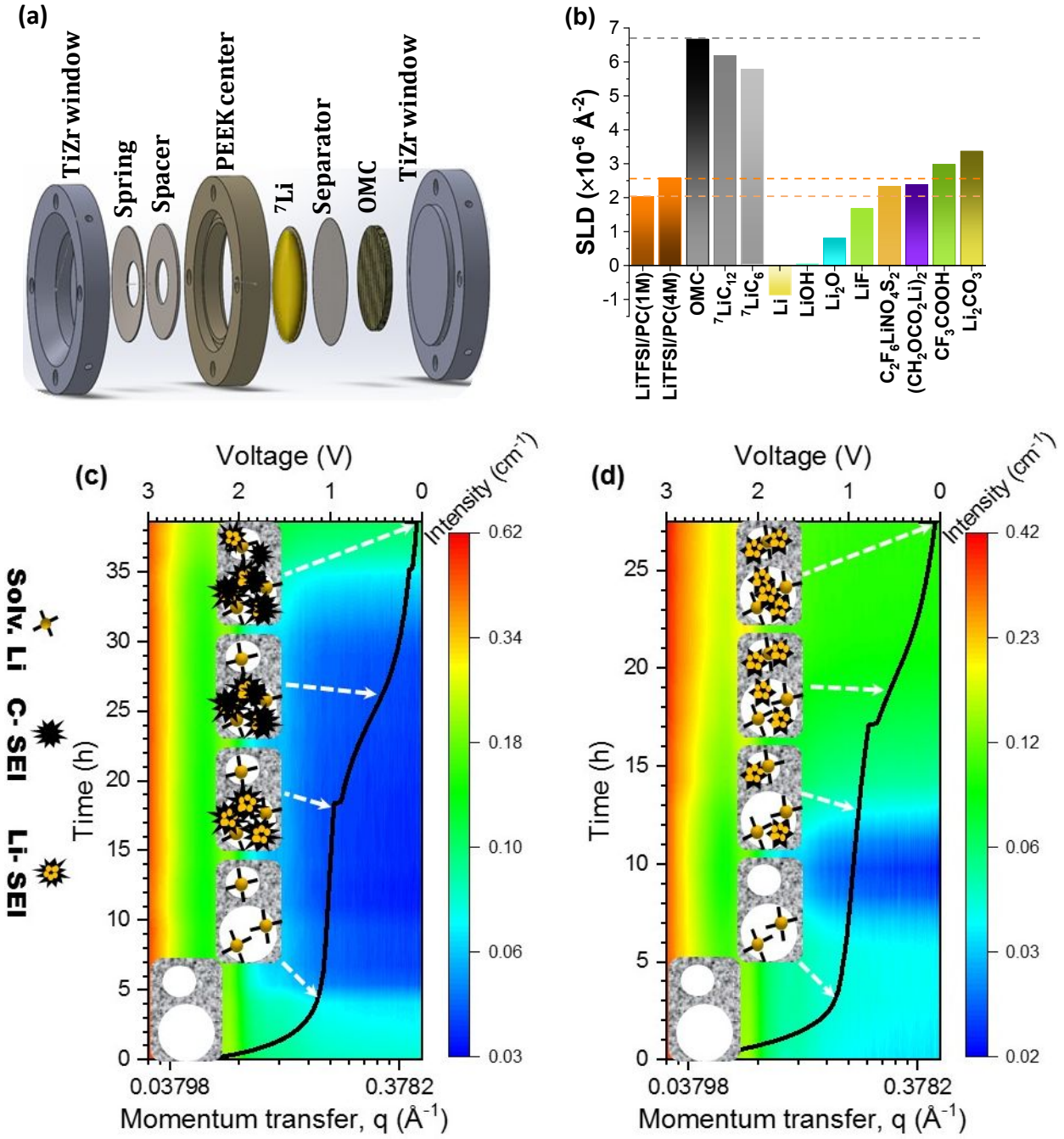

Fig. 1: (a) Schematic view of the *operando* SANS cell. (b) The scattering length density (SLD) values for dominant components present in the cell at OCV (electrolyte, carbon), and those which may form as a result of cycling (lithiated carbon, lithium) and electrolyte reduction (major SEI components). Dashed lines indicate the difference in contrast between the two electrolytes. The SANS intensity (cm^{-1}) as a function of the scattering vector q, 1st discharge time and voltage for (c) the 1 M LiTFSI/PC and (d) the 4 M LiTFSI/PC electrolyte systems. The complete raw data are shown in **Fig. S6**.

The microstructural information ranges from the Porod region at low q to the microporous region at high q, and includes more direct data on the carbon electrode expansion due to the peak from mesopore ordering. The mesopore peak position and intensity indicate the pore-pore spacing, and

the contrast between the pore and the carbon framework, respectively. The intensity decay at the low q values indicates the carbon surface fractality. The intensity at the highest q values reflects the micropore scattering intensity (contrast between the micropore and its surroundings [MPSI], and the amount of material with that contrast in the beam) and background; the background is constant, as there is little change in the total quantity of material in the beam throughout the discharge / charge of the cells [39, 49, 50]. The scattering curves scaled to absolute units are shown in **Figs. 1c** and **1d** as a function of the cycling time, and the *operando* potentiograms are superimposed on the scattering curves to highlight the relationship between state-of-charge and scattering intensities. It is clearly observed that the scattering intensities evolve over the entire q range for both the 1 M and 4 M cells, and that the data vary with electrolyte concentration.

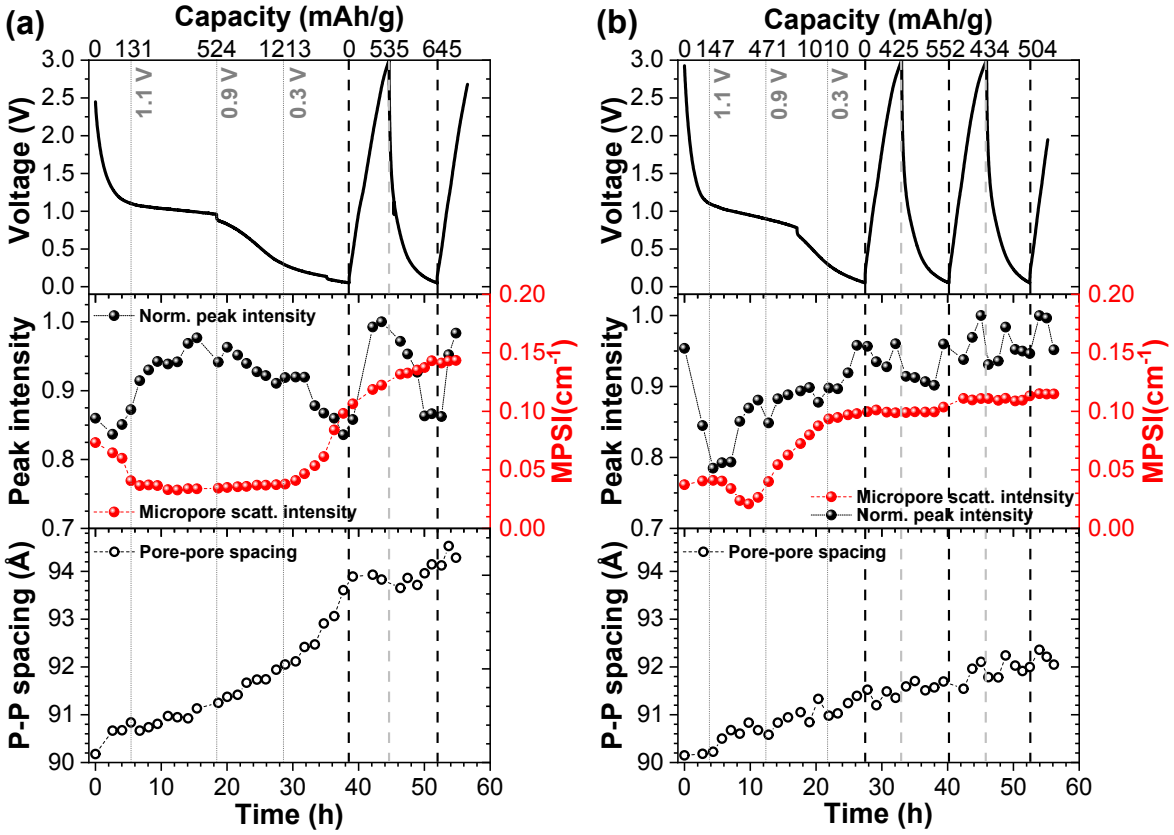

Fig. 2: *Operando* electrochemical and SANS results for (a) the 1 M and (b) the 4 M electrolyte systems. Top: electrochemical cycling profile; Middle: integrated Gaussian peak intensity for pore ordering and micropore (high q) scattering intensity (MPSI); Bottom: pore-pore spacing determined by the Gaussian peak position. See supplemental section for details of the SANS data analysis.

The SANS curves are fit with the model shown as eq. (1) in the supplemental section. The integrated peak intensity and the peak position are extracted by means of a Gaussian function, with the pore-pore spacing calculated as $2\pi/q$. The micropore scattering intensity is extracted by observing the last term of eq. (1), and is evaluated independently from the mesopore scattering. The extracted parameters are plotted as a function of discharge/charge in **Fig. 2a** for the 1 M and **Fig. 2b** for the 4 M electrolyte systems. These data allow us to assess the dynamic cell chemistry during discharge and charge over several voltage regions, through comparison with calculated scattering length density (SLD; a measure of scattering power) as shown in **Fig. 1b**.

To better understand the evolution of the surface chemistry for 1 M and 4 M electrolytes, and thereby the contrast changes in the *operando* SANS data, we have collected *ex situ* XPS data at representative voltages (OCV, 1.1V, 0.9V, 0.3V and 0.005V) during the initial discharge. These voltages were selected to coincide with changes in the trend of the electrochemical profile and/or SANS data, which are representative of changes in surface and bulk processes. **Fig. 3** shows the comparison of surface elemental concentrations on electrodes from the 1 M and 4 M electrolyte systems at different potentials. The elemental composition, in at. %, of the electrode surfaces at different potentials are presented in **Table S2**. The elements O, C, N, F, Li and S were detected on the surface of the electrodes from both electrolyte systems. It is generally accepted that the initial stage of SEI formation is a two-step process: i) during polarization of the negative electrode the components in the electrolyte undergo reductive decomposition forming new chemical species and ii) these species undergo a precipitation process and then start forming the SEI layer until all of the sites on the carbon surface are covered [51]. **Fig. 3** indicates that both the 1 M and the 4 M have somewhat similar SEI elemental compositions at specific voltages. However, there are subtle differences in the evolution of the SEI during the first discharge. The general trends are an increase in O and Li, and a decrease in C, with decreasing voltage. This is consistent with the initial formation of largely organic components, followed by an increase in inorganic Li containing compounds. However, the trends for F and S are more complex, and differ between the 1 M and 4 M cells. We will discuss the spectra in greater detail for Li, C, and F, and we find that the combination of the XPS and SANS data provides an exceptional amount of information on the cycling mechanism in different regions, as discussed below and summarized in **Table 1**.

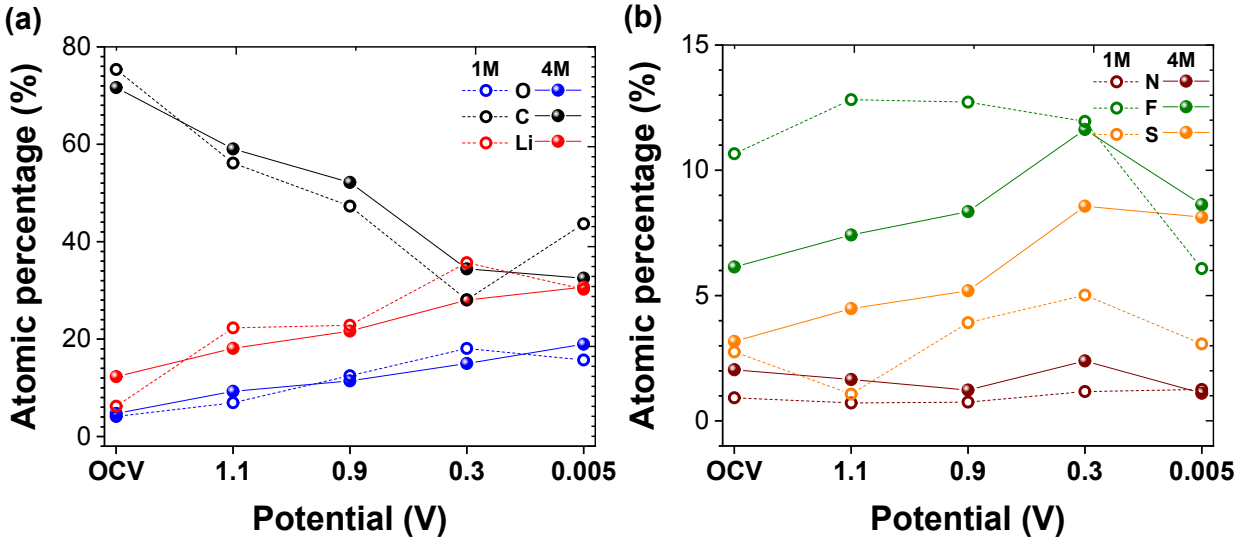

Fig. 3: Comparison of the concentrations of the surface elements (a) O, C, Li and (b) N, F, S from the 1 M and 4 M electrolyte electrodes at OCV, 1.1 V, 0.9 V, 0.3 V and at 0.005 V.

Cell chemistry during discharge from OCV to 1.1V

The voltage profile of both cells (**Fig. 2**, top) from OCV to 1.1V shows a continuous voltage drop. This behavior is characteristic of the formation of an electric double layer (EDL), which is the adsorption of ions onto the surface of the HC [43]. This part of the storage process contributes to approximately 131 mAh/g to 147 mAh/g for the 1 M and 4 M cells, respectively, in which the solvated Li^+ are adsorbed onto the pore walls of the unoccupied micro- and mesopore surfaces. For 1 M this results

in the contrast, $\Delta\rho^2$, decreasing from that of the unfilled mesopores (C vs. Ar, $\Delta\rho^2 \approx 49 \times 10^{-12}\text{Å}^{-4}$) to the contrast of that of $Li^+(PC)_4$ filled pores (C vs. $Li^+(PC)_4$, $\Delta\rho^2 \approx 16 \times 10^{-12}\text{Å}^{-4}$). For the 4 M electrolyte, the solvation shell now involves partial association of $TFSI^-$ anion, and the Li^+(PC)-TFSI aggregates are readily adsorbed onto the mesopores with a resulting decrease in the contrast between the HC framework and the mesopores, and a corresponding decrease in the mesopore peak intensity. Thus, we observe a trend of decreasing mesopore peak intensity with discharge which follows the expectation for pore filling by electrolyte that displaces Ar. For the micropores, the MPSI of the 1 M cell similarly decreases due to solvated Li^+ adsorption, while the 4 M cell MPSI is constant in this region. In the micropore case, the percentage decrease in the MPSI (0.0733 cm^{-1} to 0.0330 cm^{-1}) is nearly identical to the calculated value for the displacement of argon by solvated Li^+, indicating a 55 % decrease in the contrast and the MPSI for the 1 M cell. These data demonstrate that it is both the adsorption of ions and the displacement of Ar, driven by the electric field, that dominates the scattering intensity in this region.

In this adsorption region there is evidence for a change in the microstructure for the 1 M cell. An increase in the pore-pore spacing, from ~ 90.1 Å to ~ 90.8 Å (Δd = 0.7 Å), which indicates an increase in the unit cell and an expansion in the carbon framework. There is no corresponding change in the microstructure of the 4 M cell, just as the intensity of the MPSI is constant. It is surmised that for the 1 M the $Li^+(PC)_4$ adsorbing onto and filling the micropores causes an increase in the pore-pore spacing, due to the $Li^+(PC)_4$ complex causing stress on the micropores, whereas the 4 M cell does not show this behavior at 1.1 V. We note that according to calculations done by Shi et al. [17] the $Li^+(PC)_4$ has the maximum size of 10.19 Å, which would block the micropores, whereas aggregates in the 4 M electrolyte would have a lower coordination number and consist of smaller molecules (e.g. $Li^+(PC)_3$ has a 3.06 Å dimension). Therefore, the lack of micropore filling in the 4 M cannot be ascribed to the size of the lithium complex, but is the first indication that the higher viscosity plays a role in the electrochemical cycling mechanism, as the more viscous solution does not yet enter the micropores.

Further details can be teased out of the data in this region by noting that the peak intensity for the 1 M does not have a constant decreasing trend: it starts to increase below c.a. 1.3 V. The higher viscosity of the 4 M slows the pore filling, and it is this gradual pore filling that dominates the scattering to 1.1 V. For the 1 M cell, the increasing trend in the peak intensity from ~ 1.3 V up to ~ 1.0 V suggests that $Li^+(PC)_4$ adsorption onto the mesopores and Ar displacement no longer dominates the scattering. As the increase in the peak intensity is related to an increase in the contrast between the carbon framework and the mesopores, it could therefore be the result of either one of two scenarios: (i) the carbon framework SLD increases, or (ii) the pore SLD decreases. The former scenario cannot realistically occur within this system at these potentials (~ 1.1 V) and therefore the latter scenario is more likely the case. The most consistent explanation is that as the displacement of argon is completed, the buildup of Li on the surface begins to dominate the scattering. The XPS data indicate that the surface layer contains Li and C components at OCV, and that the Li content increases while the C content decreases during discharge for both the 1 M and 4 M electrodes. Beyond simply covering the surface with $Li^+(PC)_4$, upon partial desolvation during discharge below 1.3 V in the 1 M cell, the partially solvated Li^+ ion would have a smaller SLD and could increase the contrast. Therefore, what we are seeing through the contrast variation in this region is the entire process of pore filling, adsorption of $Li^+(PC)_4$, and the buildup in Li concentration and initial SEI formation on the HC surface.

From 1.1V to 0.9V

In this region the effects of intercalation and electrolyte decomposition to form a passivation layer dominate the scattering for the 1 M cell, and micropore filling initially plays an important role for the 4 M cell. The trend in ordered mesopore peak intensities of the two cells differ, in that the 1 M cell shows a slight increase below 1.1 V, while the intensity for the 4 M cell is initially flat before increasing rapidly as the cell potential drops below ~1.0 V. For the 1 M cell, this is the region where there is co-intercalation of fully or partially solvated Li^+ into the graphitic layers, and from ~ 1.1 V to ~ 0.9 V a plateau in the potentiogram is observed. This co-intercalation has been reported first by Besenhard et al. [52] and later confirmed by the group of Ogumi [53-55] by means of *in situ* AFM measurements. Our SLD calculations suggest that co-intercalated $Li^+(PC)_4$ would not significantly affect the SLD of the carbon framework, thus leaving the carbon framework SLD essentially constant. Given the micropore scattering would also be affected by changes in the carbon framework SLD, the constant contrast of the MPSI from OCV to ~ 0.9 V (the plateau region in the potentiogram) supports the conclusion that the framework SLD has not yet changed significantly. Though the solvated Li^+ is attracted to the surface and intercalated into graphitic layers, the $TFSI^-$ anions are not intercalated into the negatively charged electrode. Consequently, there is a build-up of $TFSI^-$ anions in the mesopores, and the Li^+ and $TFSI^-$ present at the mesopore surface reduces to form a Li and F rich SEI with chemical compounds such as Li_2O and LiF, as seen from the F 1s and Li 1s XPS spectra in **Figs. 4b** and **c**, respectively. The presence of LiOH in the XPS spectra can be ascribed to the reaction of Li with trace water in the electrolyte [51]. We note that during the first discharge the SEI typically forms in thicknesses greater than the average pore size of ~4 nm, and it is therefore likely that the SEI will fill the pore volume rather than being confined solely to the pore surface. The onset reduction potentials are expected to be high for LiTFSI (2.9 V – 2.7 V) as compared to Li^+-PC (~ 0.6 V) and PC (theoretically ~ 0.3 V and experimentally 1.6 – 1.0 V) [56, 57]. The reduced products of $TFSI^-$ have SLD's that are typically lower compared to $Li^+(PC)_4$ (see **Fig. 1b**). Therefore, SEI formation in this potential window causes an increase in the contrast between carbon framework and mesopores.

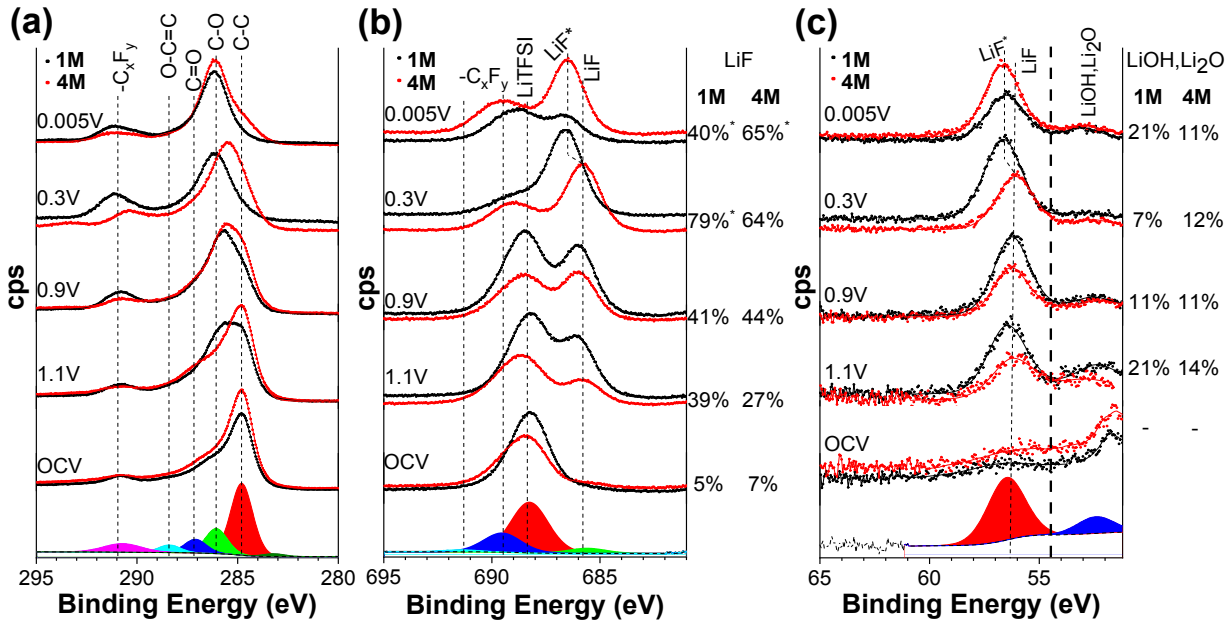

Fig. 4: The XPS spectra of (a) the C 1s peak, (b) the F 1s peak and (c) the Li 1s peak from the 1 M (black) and 4 M (red) OMC electrodes. The bottom peaks show the peak fits, as an example. *LiF is the electrochemical shifted LiF peak.

For the 4 M cell, from 1.1V to ~ 1.0 V (7.1 h) the peak intensity is constant, due to a build-up of LiTFSI on the surface that offsets the contrast change due to the remaining Ar displacement. This is also evident from the F 1s spectra at OCV and 1.1 V (**Fig. 4b**) with a prominent peak ascribed to LiTFSI (688.4 eV) [16]. The SANS peak intensity sharply increases after ~ 1.0 V until ~ 0.9 V indicating the changes in SEI chemistry on the mesopores now dominate, as pore filling is completed for the viscous 4 M electrolyte. This is the plateau region in the potentiogram that indicates co-intercalation and SEI formation. In fact, it is observed from the F 1s spectra measured at 1.1 V and 0.9 V that the peak ascribed to LiF (~686 eV) increases systematically. In addition, chemical compounds such as LiOH and Li_2O are present in the SEI as seen in **Fig. 4c**. As in the 1 M cell, it is the surface chemistry that now dominates the scattering.

For the 4 M cell, the point at which the Li^+(PC)-TFSI begins to get adsorbed onto the micropores is clear in the data. The MPSI is constant to ~ 1.0 V after which there is a decrease until a minimum at 0.95 V during adsorption, and possibly Ar displacement. Note that below 1.0V with the adsorption of the Li^+(PC)-TFSI and LiTFSI in higher quantities onto the micropores, an increase in the contrast between the C framework and the mesopores is expected; this would additionally contribute to the increase in the ordered mesopore peak intensity. We find that the adsorption requires a stronger driving force due to the higher viscosity of the 4 M electrolyte, such that the Li^+(PC)-TFSI can penetrate the micropores only at a lower potential.

As noted, in this potential range the co-intercalation of solvated Li^+ into the carbon has little effect on the contrast as compared to the surface chemistry, and the XPS spectra of F 1s and Li 1s have shown important contributions from Li salts. The C 1s spectra provide complimentary information on the surface chemistry of the organic or metal organic compounds present. **Fig. 4a** shows the C 1s spectra of the 1 M and 4 M electrodes. For both the 1 M and 4 M electrodes, a sharp peak at 284.8 eV is observed which is from the HC, and this peak is present at OCV. The peaks at 286.1 eV (C-O) and 287.2

eV (C=O) are related to ether carbons in CH_3OCO_2Li or $(CH_2OCO_2Li)_2$. The peaks at 288.4 eV (O-C=C) and ~291 eV (C-F) are related to O-C=C and C-F bonds, respectively, and the ~291 eV peak also contains satellite peaks which broaden the FWHM. From 1.1V and below, the peak at 286.1 eV, which is related to C-O containing species, increases at a faster rate for the 1 M electrode as compared to that of the 4 M. This indicates a faster PC reducing to SEI components for the 1 M electrode. Similarly, the peaks at ~291 eV related to the C-F bonds can be seen increasing with decreasing potential for the 1 M electrode where for the 4 M electrode the peak stays broadened and do not increase substantially. This indicates an increased and higher C-F content for the 1 M electrode as compared to the 4 M electrode, and supports the more rapid formation of organic components in the 1 M cell.

The pore-pore spacing shows concentration dependent effects on the HC microstructure related to micropore filling. The 1 M electrode experiences a relatively small expansion from ~ 90.8 Å to ~ 91.2 Å (Δd = 0.4 Å), whereas the 4 M electrode shows an initial jump in spacing to ~ 90.8 Å (Δd = 0.7 Å) related to the filling of the micropores, followed by relatively little change. This expansion of the HC framework for the 4 M electrode is nearly identical to that occurred in the 1 M electrode at higher voltage. We note that in both cases the shift in ordered mesopore peak position precedes the increase in peak intensity, suggesting that the co-intercalation and SEI formation are aided by the expansion. Overall, we find that within this electrochemical window the higher viscosity of the 4 M electrolyte has played a major role in shifting the HC framework expansion to lower voltages, and the higher concentration has resulted in a slower formation of organic SEI components with respect to the 1 M electrolyte.

From 0.9V to 0.3V

In this region the neutron scattering for the 1 M cell is dominated by changes in surface chemistry of the mesopore, while for the 4 M cell there are again important changes in the micropore scattering. The ordered mesopore peak intensity of the 1 M cell shows a continuous decrease, while the intensity for the 4 M cell marginally increases. For the 1 M cell from ~ 0.9V to ~0.3V a sloping region in the potentiogram is observed, and there are definite changes in the composition of the SEI. The downward trend of the mesopore peak intensity can be explained by the fact that PC and Li^+-PC reduce at lower potentials to form a more carbonaceous SEI with chemical compounds such as $ROCO_2Li$ compounds. This is seen from the C 1s XPS spectra (see **Fig. 4a**) measured at 0.9 V and 0.3 V where, for example the peak intensity of the peaks at E_{BE} ~291 eV increases indicating the presence of increased C-F content, which has a relatively high SLD (see **Fig. 1b**). Also, the C-C peak reduces in intensity with an increased presence of $ROCO_2Li$ compounds. These compounds, as shown in **Fig. 1b**, have higher SLD values as compared to the Li-rich compounds causing the decrease in the peak intensity up to ~ 0.3 V (t = 28.6 h), and dominate over the scattering contribution from inorganic components such as LiF. Despite significant changes for the mesopore scattering in the 1M cell, the MPSI shows only a slight increase. This increase in the MPSI is due to the small increase of the SLD of the carbon framework caused by the continuous co-intercalation of solvated Li into graphitic layers, while the composition of the micropore itself does not change significantly. In effect, the higher HC SLD increases the contrast between the carbon framework and the micropore resulting in the slight MPSI increase.

However, for the 4 M cell, there is evidence for a significant change in the chemical composition of the micropores. The MPSI starts to show a sharp and dramatic increase below ~ 0.95 V until ~ 0.3 V. In this voltage range the potentiogram shows a sloping discharge. The increase in the MPSI is a result of an increase in the concentration of Li in the micropores, which decreases its SLD. Furthermore, the

decrease in the micropore SLD causes the SLD of the C framework to decrease with respect to the pore. From the XPS measurements, taken at 0.9 V and 0.3 V, it is seen from the F 1s spectra (see **Fig. 4b**) there is an increase in the LiF content. At the same time carbonaceous fluorene ($-C_xF_y$) starts to form as is evident from the increase in the peak ascribed to $-C_xF_y$ (~291 eV). These compounds (e.g., LiF and $-C_xF_y$) are a mixture of relatively low and high SLD's. This mixture will increase the SLD in the mesopore due to the increase in $-C_xF_y$ (see **Fig. 1b**), and combined with the decrease in the SLD of the C framework from micropore filling, causes a slight increase in the overall mesopore peak intensity from ~0.9 V until 0.3 V. These data reveal how a complex process of SEI formation and micropore filling is occurring in the HC.

The pore-pore spacing from 0.9V to 0.3V shows a more significant increase from ~ 91.2 Å to ~ 92.1 Å (Δd = 0.9 Å) for the 1M cell, and ~ 90.5 Å to ~ 91.0 Å (Δd = 0.5 Å) for the 4M cell. The more rapid increase in pore-pore spacing for the 1M is likely caused by the larger size of the PC solvated Li^+ cation [17] as compared to the Li^+(PC)-TFSI aggregates in the 4M solvent: similar levels of co-intercalation or micropore filling would produce a smaller expansion of the HC framework in the 4M cell.

From 0.3V to the lower discharge limit

Within the final discharge region to the low voltage cutoff the SANS data for the 1 M cell now exhibit large changes in the micropore scattering, while for the 4 M cell the micropore scattering ceases to change significantly and the mesopore scattering increases strongly. The mesopore peak intensity for the 1 M cell continues with an overall downward trend until the end of the first discharge, and is again related largely to the SEI surface contributions. From the C 1s spectrum (see **Fig. 4a**) there is a shift in the peaks to the higher binding energy indicating an increase in the presence of C-O, C-O-C and O-C=C chemical compounds [58,59]. From the C 1s and F 1s spectra (see **Figs. 4a** and **b**) the presence of $-C_xF_y$ containing compounds increased from 0.3 V (~ 6%) to 0.005 V (~17%). These $-C_xF_y$ compounds have quite high SLDs that are above the SLD of the electrolyte. In **Fig. 4b** the F 1s spectrum shows that LiF content increases to a maximum at 0.3 V, before decreasing to 0.005 V due to a relatively thick layer of carbonaceous compounds. It should also be noted that from the Li 1s spectra that there is an increase, from 0.3 V to 0.005 V, in the presence of Li-rich compounds (LiOH and Li_2O) having lower SLDs than the electrolyte. Finally, the possible intercalation of partially desolvated Li^+ at lower voltages can decrease the SLD of the carbon framework. Given the presence of both higher and lower SLD components, we see from the downward trend in mesopore peak intensity for the 1 M that the scattering is dominated by organic components on the surface, possibly with a contribution from Li^+ intercalation into the HC framework.

For the 1 M cell, a sudden increase (~ 15%) in the MPSI is observed from ~ 0.3 V to the end of the first discharge. This indicates that there is a dramatic change in either the SLD of the carbon framework or the micropores. At the low voltage part of the potentiogram, it has been suggested that "nano voids" in the HC, the micropores in this case, will be filled with Li [37]. With the negative SLD of Li, the contrast between the carbon framework and the micropores increases drastically from a contrast between C vs. $Li^+(PC)_4$ ($\Delta\rho^2 = 17 \times 10^{-12}$ Å^{-4}) to C vs. Li ($\Delta\rho^2 = 50 \times 10^{-12}$ Å^{-4}), with the assumption that < 2nm Li particles fill the micropores. We find that when the percentage increase for both the experimentally obtained MPSI in cm^{-1} and the calculated contrast values in Å^{-4} are compared, similar values of 181 % and 194% for the MPSI and the contrast, respectively, are obtained. When considering some contribution of intercalation to the decrease in the SLD of the HC framework, and the possibility of low SLD Li salts forming in the micropores, we find that the change

in MPSI is best described by a strong contribution from buildup of Li-rich compounds in the micropores at a lower voltage than for the 4 M electrolyte.

In the case of the 4M cell, there are no signs in the XPS spectra of dramatic increases in the lower SLD SEI components on the HC surface. This is unexpected, given that there are few options to explain the observed increase in the mesopore peak intensity in this potential region. It was previously considered that volume expansion of the carbon could lead to a larger peak area due to an increase in the quantity of material scattering from the pores, but this cannot explain the 4M cell as there is little volume expansion in this region [43]. A second option could be a large increase of the framework density during co-intercalation, but the overall trend in the peak intensities during the discharge again do not agree with this. Therefore, the increase in the mesopore peak intensity observed from 0.3 V until the end of the first discharge must be due to low SLD Li species increasingly dominating the micropore scattering. While the higher Li concentration is not directly shown by the XPS data, it may be that the organic layer on the SEI at lower voltages is masking an increasing quantity of Li salt SEI components in the mesopores (e.g., LiF, LiOH). The MPSI starts to level off at ~ 0.3 V until the end of the first discharge; this points to a saturation of the available micropores during the process of low SLD Li deposition, and implies that the micropores are playing less of a role in the chemistry of the cell after the end of the first discharge.

The XPS data hint at the nature of the SEI layer that forms in the two cells. The relatively weak peak intensity of the HC electrode, for the 1 M electrode as compared to the 4 M electrode, at 284.8 eV in the 0.005 V spectra indicates that the SEI layer is thicker for the 1 M electrode. In addition, the relative Li content increases in an irregular manner for the 1 M electrode, with the apparent highest value at 0.3 V (36 at. %) before reducing at 0.005 V (30 at. %). The irregular Li content as a function of the discharge indicates that the Li rich layer forming on the 1 M electrode is inconsistent with a higher carbonaceous content. However, the C content for the 4 M electrode shows little change from 0.3 V (34 at. %) to 0.005 V (33 at. %) and that of the 1 M electrode shows an increase from 28 at. % to 44 at. % in this voltage range.

The pore-pore spacing in the 1 M cell shows higher slope at low voltages, increasing from ~ 92.1 Å to ~ 93.9 Å (Δd = 1.8 Å), corresponding to the change in the MPSI and further solvated Li co-intercalation. However, the 4 M cell did not show the same rapid increase during the low SLD Li intercalation (or aggregation) in the micropores at higher voltages. In fact, the pore-pore spacing of the 4 M cell increased slightly from ~ 90.2 Å to ~ 91.4 Å (Δd = 1.2 Å) during the entire discharge. The difference can be related to the smaller solvated Li^+(PC) and even naked Li^+ adsorbing onto and filling the micropores, as compared to more fully solvated Li^+ in the 1M electrolyte. An expansion at low voltages has been reported by Besenhard et al. [52], involving a > 150 % expansion at potentials lower than 1.0 V vs. Li^+ in their 1 M $LiClO_4$/EC-DMC electrolyte with highly ordered pyrolytic graphite (HOPG) as working electrode. Also, the group of Ogumi [53-55] showed by *in situ* AFM that with co-intercalation there is a concomitant hill-like formation, in their case, on the basal plane of HOPG that was used as working electrode in different electrolyte systems. However, the expectation has long been that HC were essentially rigid during cycling, and this type of expansion has only recently been shown using *operando* SANS data [43]. In this work, the new argument can be made that the micropore filling exerts stress on the framework and is equally responsible for the expansion of the HC framework in the first discharge.

Table 1: A comparative summary of the 1 M and 4 M LiTFSI/PC electrolyte cell chemistry during the first discharge.

	Dilute electrolyte (1 M)	Concentrated electrolyte (4 M)
	EDL formation	
OCV – 1.1V	❑ $Li(PC)_4$ adsorbed onto micro- and mesopores, along with Ar displacement to fill the pores. ❑ LiF content higher compared to 4 M, and increasing with discharge. ❑ Pore-pore spacing increases with $\Delta d = 0.7$Å from adsorption into pores.	❑ Li(PC)-TFSI aggregates adsorbed onto mesopores only, due to high electrolyte viscosity. ❑ LiF content lower compared to 1 M, and increasing with discharge. ❑ Pore-pore spacing is constant.
	Voltage plateau / Co-intercalation	
1.1V – 0.9V	❑ $Li^+(PC)_4$ has filled the micropores and does not yet reduce significantly. ❑ LiTFSI starts to reduce, forming Li rich SEI in the mesopores. Carbonaceous compounds (e.g., C-O, C-F) increase as PC begins to decompose. ❑ Pore-pore spacing increases gradually with $\Delta d = 0.4$Å due mainly to co-intercalation.	❑ Li(PC)-TFSI fills the micropores below 1.1V. ❑ LiTFSI starts reducing at lower voltage, forming Li rich SEI (i.e., LiOH, Li_2O, LiF) in the mesopores. Less carbonaceous compounds present in SEI relative to 1 M electrode. ❑ Pore-pore spacing shows an increase of $\Delta d = 0.7$Å due to adsorption into pores.
	Sloping discharge	
0.9V – 0.3V	❑ The composition of the filled micropores has not changed from $Li^+(PC)_4$. ❑ Carbonaceous compounds in the mesopores begin to dominate the scattering over Li rich compounds. ❑ The expansion of the C framework is high with $\Delta d = 0.8$Å due to co-intercalation of the larger solvated Li^+ species.	❑ Micropores are being filled with Li-rich phases, at much higher potentials as compared to the 1M. ❑ Changes in the SEI chemistry are partially offset by co-intercalation and pore filling, resulting in small overall contrast changes. ❑ Expansion rate of C framework is relatively small with $\Delta d = 0.4$Å.
	Low voltage plateau	
0.3V – 0.05V	❑ Micropores are being filled with Li-rich compounds. ❑ The mesopore scattering is dominated by carbonaceous compounds.	❑ Micropores have become saturated with Li-rich compounds. ❑ The mesopore scattering is dominated by low SLD Li-rich compounds (Li salts).

	❑ The SEI is thicker than the 4 M electrode. ❑ The expansion rate of C framework is very high with $\Delta d = 1.6$Å, due to pore filling and co-intercalation.	❑ The presence of carbonaceous compounds in the SEI is evident, though minute. ❑ The expansion rate of C the framework remains gradual with $\Delta d = 0.5$Å.
Δd_{total}	$\Delta d = 3.5$Å	$\Delta d = 1.4$Å

Subsequent charge and discharge cycles

Following the unique chemistry presented by the SEI formation and HC expansion in the first discharge, the subsequent charge/discharge cycles provide an important comparison. For the 1M cell, the first charge (Li^+ de-intercalation) profile shows mostly a sloping charge up to 3.0 V with no clear plateau, which indicates that Li de-intercalation from graphitic layers does not occur to a significant extent. The sloping profile is also observed in the *ex situ* electrochemical potentiograms, and in subsequent charge/discharge cycles. The increase/decrease in the mesopore peak intensity during charge/discharge is consistent with desorption/adsorption of solvated Li ions that did not take part in the reduction process. However, the increase in the micropore intensity in the first charge cycle, while also consistent with solvated Li desorption, is not found to be reversible. Given the common finding that the SEI experiences relatively little change after the initial discharge, it is likely that the micropores largely contain reduction product, while the mesopores may contain some unreduced solvent available for Li^+ desorption. Corresponding to the intensity changes in the mesopore peak, it is evident in the region from the first charge to the second discharge that the contraction and expansion in the carbon framework shows a small reversibility with a pore-pore spacing between ~ 93.9 Å and ~ 94.2 Å (Δd = 0.3 Å). As suggested above the solvated Li exerts stress on the micropores when filling and the framework relaxes during the charge process.

As with the 1 M electrolyte system, the potentiogram for the 4 M cell has a mostly sloping region without any significant sign of a plateau, suggesting little Li deintercalation occurs. The MPSI do not show significant changes during the subsequent charge and discharge profiles, though it can be argued that during the first and second charges the MPSI shows a slight increment. This suggests a small fraction of the species in the micropores can be reversibly inserted. This is consistent with the pore-pore spacing which shows a constant increasing trend, however small. The mesopore peak intensity in the subsequent charge and discharge processes does not show any clear trends. This could be the result of continual SEI formation because of the large surface area of the HC, consistent with the ex-situ cycling results on increasing coulombic efficiency with cycling in the first 10 cycles.

Cell impedance and interfacial passivation

Electrochemical impedance spectroscopy data were collected at several voltages, and are useful to compare against expected changes in interfacial passivation during the initial discharge. **Fig. S7** shows the *in-situ* EIS derived data, the R_Ω, R_{SEI} and the R_{ct}, of the 1 M and 4 M electrolyte systems as a function of the discharge. These are the electrolyte resistance (R_Ω), the resistance from the interfacial passivation layer (R_{SEI}) and the charge-transfer resistance (R_{ct}). The R_Ω shows a clear increase in resistance for the 4 M electrolyte system as compared to that of the 1 M, due to the lower conductivity of the 4 M electrolyte, consistent with previous reports. [6, 17] The R_{ct}, from OCV to ~ 1.1 V, for the 1 M

and 4 M electrolyte systems displays an increase which is indicative of the evolution of a SEI layer with insulating properties, and is consistent with the increase in LiF content within this voltage region observed in the XPS data. We note that the increase in the 4 M electrolyte system is much steeper as compared to that of the 1M electrolyte system which can be explained by a more lower conductive inorganic layer forming on the 4 M electrode. The R_{ct} for the 1M system reaches a maximum at a voltage just below 1.1 V and decreases. At this voltage region it is shown by SANS and XPS that a carbonaceous SEI is starting to dominate on the 1M electrode. The carbonaceous SEI is a better conductor and thus a decrease in the R_{ct} is expected. The R_{ct} for the 4 M system shows a gradual increase up to ~ 0.6 V where a maximum is reached after which a slight decreasing trend is observed, and similar results are observed for R_{SEI}. This is consistent with a relatively stable SEI layer forming, as also suggested by the mesopore peak intensity in the SANS data. The R_{SEI} of the 1 M cell displays a different behavior. It increases only at ~ 0.9 V where a thicker carbonaceous SEI is expected; in this case the thickness of the SEI may be playing a more dominant role than the intrinsic conductivity on the measured resistance. These EIS data confirm the formation of the SEI composition during the initial discharge, and suggest that a more uniform SEI layer is formed for the concentrated electrolyte.

Conclusions

Similar mechanisms of adsorption, pore filling, SEI formation and intercalation are occurring in the 1 M and 4 M electrolytes, but there are major differences in when these mechanisms dominate as a function of voltage. There are several key findings from this work with implications for the use of concentrated electrolytes. Firstly, the viscosity of the electrolyte has a major influence on pore filling, and higher viscosity can thereby displace electrochemical processes to lower voltages. We see similar expansion of the carbon framework in the 1 M and 4 M cells due to micropore filling, but this expansion occurs just below OCV in the 1 M cell and below 1.1V in the 4 M cell. The size of the solvation shell around Li^+ is found to influence framework expansion during the first discharge, with the larger PC coordinated Li^+ in 1 M electrolyte producing an overall 3.5 Å (~4%) increase in the pore-pore separation relative to the 1.4 Å (~1.5%) increase for the Li(PC)-TFSI aggregates; this is due to a combination of pore filling and co-intercalation into graphitic layers.

Both 1 M and 4 M electrolyte systems show EDL formation by adsorption of solvated PC to the electrode surface. In the 1 M electrolyte system it is known that the inner Helmholtz layer is dominated by free PC molecules and that of the 4 M by salt anions [9]. Despite the prevalence of PC in the inner Helmholtz layer of the 1 M electrolyte system, the TFSI- anions present at the anode surface begin to reduce at a higher potential and at a faster rate as compared to the PC, due to the higher reduction potential of the -TFSI anions. We find that Li-rich salts (i.e., LiF, LiOH, Li_2O) form at higher voltages for the 1 M electrolyte, but that in the sloping discharge region of 1.1V-0.9V the salts begin to dominate the mesopore scattering for the 4 M electrolyte, while carbonaceous products (e.g., C-O, C-F containing compounds) begin to dominate for the 1 M electrolyte. Despite the fact that filling of the micropores occurs at lower voltages in the 4 M electrode, the reaction to form Li-rich reduction products begins immediately upon pore filling (~0.95V); meanwhile, the composition of the $Li^+(PC)_4$ filled micropores remains stable in the 1 M electrolyte down to lower voltages (~0.3V), due to the relative lack of available $TFSI^-$ to promote Li-rich products. By the end of the first discharge the 4 M electrolyte has a passivation layer richer in low SLD Li-rich reduction products than the 1 M electrolyte. In combination with EIS and XPS data we find that the SEI of the 1M is thicker than in the 4 M case, mostly due to the higher PC reduction. Finally, with the subsequent charges and discharges PC or solvated PC is desorbed (charge) and adsorbed (discharge), which is shown to have significant

reversibility in the mesopores but not in the micropores. As we have shown, *operando* SANS studies can provide knowledge about the dynamic cell chemistry that is microstructure specific in new candidate electrolyte systems for high-energy density batteries, which cannot be seen from other probes such as electrochemical cycling or XPS studies. This approach has the capability to impact a wide range of electrochemical systems, taking advantage of the unique contrast provided by neutron scattering.

References

1. J. J. Xu, Z. L. Wang, D. Xu, L. L. Zhang and X. B. Zhang, *Nat Commun*, 2013, **4**, 2438.
2. Y. B. Yin, J. J. Xu, Q. C. Liu and X. B. Zhang, *Adv Mater*, 2016, **28**, 7494-7500.
3. J.-L. Ma, F.-L. Meng, D. Xu and X.-B. Zhang, *Energy Storage Materials*, 2017, **6**, 1-8.
4. D. Xu, Z. L. Wang, J. J. Xu, L. L. Zhang and X. B. Zhang, *Chem Commun (Camb)*, 2012, **48**, 6948-6950.
5. K. Xu, *Chemical Reviews*, 2004, **104**, 4303-4418.
6. Y. Yamada and A. Yamada, *Journal of The Electrochemical Society*, 2015, **162**, A2406-A2423.
7. D. Aurbach, Y. Talyosef, B. Markovsky, E. Markevich, E. Zinigrad, L. Asraf, J. S. Gnanaraj and H.-J. Kim, *Electrochimica Acta*, 2004, **50**, 247-254.
8. M. Kerner, N. Plylahan, J. Scheers and P. Johansson, *Phys Chem Chem Phys*, 2015, **17**, 19569-19581.
9. J. Zheng, J. A. Lochala, A. Kwok, Z. D. Deng and J. Xiao, *Adv Sci (Weinh)*, 2017, **4**, 1700032.
10. S. S. Zhang and T. R. Jow, *Journal of Power Sources*, 2002, **109**, 458-464.
11. Y. Yamada, C. H. Chiang, K. Sodeyama, J. Wang, Y. Tateyama and A. Yamada, *ChemElectroChem*, 2015, **2**, 1687-1694.
12. K. Matsumoto, K. Inoue, K. Nakahara, R. Yuge, T. Noguchi and K. Utsugi, *Journal of Power Sources*, 2013, **231**, 234-238.
13. X. B. Cheng, R. Zhang, C. Z. Zhao and Q. Zhang, *Chem Rev*, 2017, **117**, 10403-10473.
14. F. Sun, M. Osenberg, K. Dong, D. Zhou, A. Hilger, C. J. Jafta, S. Risse, Y. Lu, H. Markötter and I. Manke, *ACS Energy Letters*, 2018, DOI: 10.1021/acsenergylett.7b01254, 356-365.
15. S.-K. Jeong, M. Inaba, Y. Iriyama, T. Abe and Z. Ogumi, *Journal of Power Sources*, 2008, **175**, 540-546.
16. Y. Pan, G. Wang and B. L. Lucht, *Electrochimica Acta*, 2016, **217**, 269-273.
17. P. C. Shi, M. Lin, H. Zheng, X. D. He, Z. M. Xue, H. F. Xiang and C. H. Chen, *Electrochimica Acta*, 2017, **247**, 12-18.
18. S. Jiao, X. Ren, R. Cao, M. H. Engelhard, Y. Liu, D. Hu, D. Mei, J. Zheng, W. Zhao, Q. Li, N. Liu, B. D. Adams, C. Ma, J. Liu, J.-G. Zhang and W. Xu, *Nature Energy*, 2018, DOI: 10.1038/s41560-018-0199-8.
19. Z. Zeng, V. Murugesan, K. S. Han, X. Jiang, Y. Cao, L. Xiao, X. Ai, H. Yang, J.-G. Zhang, M. L. Sushko and J. Liu, *Nature Energy*, 2018, **3**, 674-681.
20. A. von Wald Cresce, O. Borodin and K. Xu, *The Journal of Physical Chemistry C*, 2012, **116**, 26111-26117.
21. D. Brouillette, D. E. Irish, N. J. Taylor, G. r. Perron, M. Odziemkowski and J. E. Desnoyers, *Physical Chemistry Chemical Physics*, 2002, **4**, 6063-6071.
22. D. M. Seo, O. Borodin, S.-D. Han, Q. Ly, P. D. Boyle and W. A. Henderson, *Journal of The Electrochemical Society*, 2012, **159**.
23. X. R. Liu, L. Wang, L. J. Wan and D. Wang, *ACS Appl Mater Interfaces*, 2015, **7**, 9573-9580.
24. Y. Yamada, Y. Koyama, T. Abe and Z. Ogumi, *The Journal of Physical Chemistry C*, 2009, **113**, 8948-8953.
25. M. Nie, D. P. Abraham, D. M. Seo, Y. Chen, A. Bose and B. L. Lucht, *The Journal of Physical Chemistry C*, 2013, **117**, 25381-25389.
26. Y. Yamada, K. Furukawa, K. Sodeyama, K. Kikuchi, M. Yaegashi, Y. Tateyama and A. Yamada, *J Am Chem Soc*, 2014, **136**, 5039-5046.
27. K. Sodeyama, Y. Yamada, K. Aikawa, A. Yamada and Y. Tateyama, *The Journal of Physical Chemistry C*, 2014, **118**, 14091-14097.
28. K. Fujii, H. Wakamatsu, Y. Todorov, N. Yoshimoto and M. Morita, *The Journal of Physical Chemistry C*, 2016, **120**, 17196-17204.
29. Y. Lu, Z. Tu and L. A. Archer, *Nat Mater*, 2014, **13**, 961-969.

30. Y. Yamada, K. Usui, C. H. Chiang, K. Kikuchi, K. Furukawa and A. Yamada, *ACS Appl Mater Interfaces*, 2014, **6**, 10892-10899.
31. K. Leung, F. Soto, K. Hankins, P. B. Balbuena and K. L. Harrison, *The Journal of Physical Chemistry C*, 2016, **120**, 6302-6313.
32. J. R. Dahn, *Physical Review B*, 1991, **44**, 9170-9177.
33. T. Ohzuku, *Journal of The Electrochemical Society*, 1993, **140**.
34. M. Inaba, *Journal of The Electrochemical Society*, 1995, **142**.
35. J. Yang, S. Muhammad, M. R. Jo, H. Kim, K. Song, D. A. Agyeman, Y. I. Kim, W. S. Yoon and Y. M. Kang, *Chem Soc Rev*, 2016, **45**, 5717-5770.
36. S. Flandrois and B. Simon, *Carbon*, 1999, **37**, 165-180.
37. M. Nagao, C. d. Pitteloud, T. Kamiyama, T. Otomo, K. Itoh, T. Fukunaga, K. Tatsumi and R. Kanno, *Journal of The Electrochemical Society*, 2006, **153**.
38. D. A. Stevens and J. R. Dahn, *Journal of The Electrochemical Society*, 2001, **148**.
39. C. J. Jafta, A. Petzold, S. Risse, D. Clemens, D. Wallacher, G. Goerigk and M. Ballauff, *Carbon*, 2017, **123**, 440-447.
40. J. Conard and P. Lauginie, *Tanso*, 2000, **2000**, 62-70.
41. T. Fukutsuka, R. Kokumai, H.-Y. Song, S. Takeuchi, K. Miyazaki and T. Abe, *Journal of The Electrochemical Society*, 2016, **164**, A48-A53.
42. C. A. Bridges, X.-G. Sun, J. Zhao, M. P. Paranthaman and S. Dai, *The Journal of Physical Chemistry C*, 2012, **116**, 7701-7711.
43. C. A. Bridges, X.-G. Sun, B. Guo, W. T. Heller, L. He, M. P. Paranthaman and S. Dai, *ACS Energy Letters*, 2017, **2**, 1698-1704.
44. S. Jun, S. H. Joo, R. Ryoo, M. Kruk, M. Jaroniec, Z. Liu, T. Ohsuna and O. Terasaki, *Journal of the American Chemical Society*, 2000, **122**, 10712-10713.
45. C. Liang, Z. Li and S. Dai, *Angew Chem Int Ed Engl*, 2008, **47**, 3696-3717.
46. A. V. Dobromyslov and N. I. Taluts, *Phys. Met. Metallogr.*, 1987, **63**, 114-120.
47. C. J. Glinka, J. G. Barker, B. Hammouda, S. Krueger, J. J. Moyer and W. J. Orts, *Journal of Applied Crystallography*, 1998, **31**, 430-445.
48. E. Frackowiak and F. Béguin, *Carbon*, 2002, **40**, 1775-1787.
49. A. Petzold, A. Juhl, J. Scholz, B. Ufer, G. Goerigk, M. Froba, M. Ballauff and S. Mascotto, *Langmuir*, 2016, **32**, 2780-2786.
50. J. Scholz, B. Kayaalp, A. C. Juhl, D. Clemens, M. Fröba and S. Mascotto, *ACS Energy Letters*, 2018, DOI: 10.1021/acsenergylett.7b01238, 387-392.
51. S. J. An, J. Li, C. Daniel, D. Mohanty, S. Nagpure and D. L. Wood, *Carbon*, 2016, **105**, 52-76.
52. J. O. Besenhard, M. Winter, J. Yang and W. Biberacher, *Journal of Power Sources*, 1995, **54**, 228-231.
53. M. Inaba, Z. Siroma, A. Funabiki, Z. Ogumi, T. Abe, Y. Mizutani and M. Asano, *Langmuir*, 1996, **12**, 1535-1540.
54. S.-K. Jeong, M. Inaba, T. Abe and Z. Ogumi, *Journal of The Electrochemical Society*, 2001, **148**.
55. T. Abe, Y. Mizutani, N. Kawabata, M. Inaba and Z. Ogumi, *Synthetic Metals*, 2001, **125**, 249-253.
56. L. Suo, O. Borodin, T. Gao, M. Olguin, J. Ho, X. Fan, C. Luo, C. Wang and K. Xu, *Science*, 2015, **350**, 938-943.
57. J. M. Vollmer, L. A. Curtiss, D. R. Vissers and K. Amine, *Journal of The Electrochemical Society*, 2004, **151**.
58. P. Verma, P. Maire and P. Novák, *Electrochimica Acta*, 2010, **55**, 6332-6341.
59. D. Aurbach, B. Markovsky, I. Weissman, E. Levi and Y. Ein-Eli, *Electrochimica Acta*, 1999, **45**, 67-86.

Acknowledgements

This work was supported by the U.S. Department of Energy, Office of Science, Basic Energy Sciences, Materials Sciences and Engineering Division. Access to the NGB 30m SANS instrument was provided by the Center for High Resolution Neutron Scattering, a partnership between the National Institute of Standards and Technology and the National Science Foundation under Agreement No. DMR-1508249. This manuscript has been authored by UT-Battelle, LLC under Contract No. DEAC05-00OR22725 with the U.S. Department of Energy. The United States Government retains and the publisher, by accepting the article for publication, acknowledges that the United States Government retains a nonexclusive, paid-up, irrevocable, worldwide license to publish or reproduce the published form of this manuscript, or allow others to do so, for United States Government purposes. The Department of Energy will provide public access to these results of federally sponsored research in accordance with the DOE Public Access Plan (http://energy.gov/downloads/doe-public-access-plan).